SUPPLEMENTARY INFORMATION

Consequences of Product Inhibition in the Quantification of Kinetic Parameters

James W. Harris[#], Anuj A.Verma, Jeremy W. Arvay, Arthur J. Shih, W. Nicholas Delgass[*], and Fabio H. Ribeiro[*]

Charles D. Davidson School of Chemical Engineering, Purdue University, 480 Stadium Mall Drive, West Lafayette, IN 47907, USA.

[#] Current address: *Department of Chemical and Biological Engineering, The University of Alabama, 3043 H. M. Comer Hall, 245 7th Avenue, Tuscaloosa, AL 35487, USA.*

*Corresponding authors: delgass@purdue.edu, fabio@purdue.edu

Table of Contents

S.1. Elemental Analysis

Table S.1. Bulk elemental analysis of Si, Al, and Cu content in Cu-SSZ-13 catalysts measured using atomic absorption spectroscopy (AAS). Data for all samples except that with Cu wt% 7.40 were originally reported in Verma et al. [1].

Si:Al	Cu wt%	Cu:Al
4.5	0.00	0.00
4.3	0.31	0.02
4.3	0.82	0.04
4.5	1.74	0.09
4.5	3.04	0.16
4.5	3.75	0.20
4.5	5.64	0.31
4.5	6.39	0.35
4.5	7.40	0.39
4.5	18.93	1.60

S.2. X-ray Diffraction (XRD) Patterns

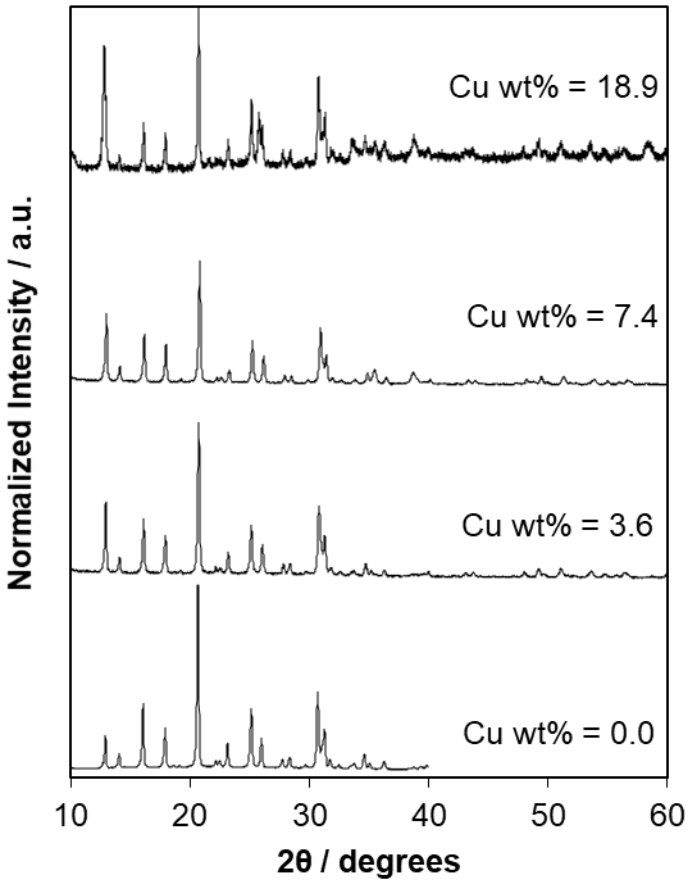

Figure S.1. Ambient XRD patterns from 10° to 60° 2θ on Cu-SSZ-13 Si:Al = 4.5 with Cu wt% of 3.6, 7.4, and 18.9, and H-SSZ-13. All Cu-SSZ-13 materials were Si:Al = 4.5 and were calcined after Cu-exchange then cooled and exposed to ambient air prior to collecting ambient XRD spectra.

S.3. Sample Ar Isotherms

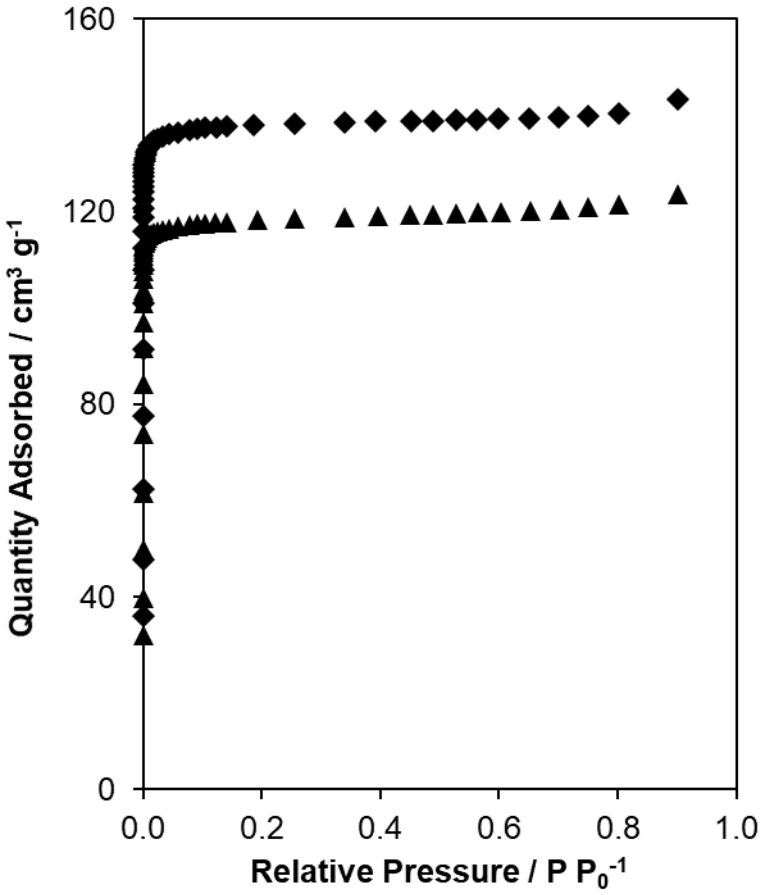

Figure S.2. Argon adsorption isotherms (87 K) of H-SSZ-13 (diamonds) and Cu-SSZ-13 (Cu wt% = 3.75, triangles)). Both samples are Si:Al = 4.5.

S.4. Diffuse Reflectance UV-Visible-NIR

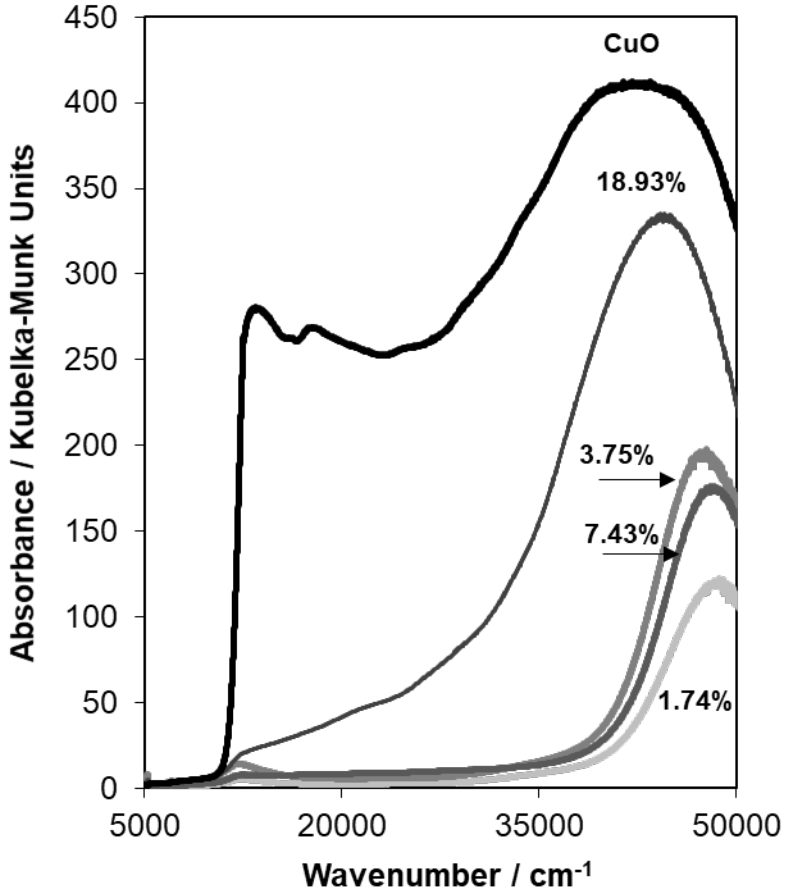

Figure S.3. Diffuse reflectance UV-visible spectra of Cu-SSZ-13 samples with Cu wt% ranging from 1.74-18.93 and of CuO, collected under ambient conditions (298 K, ambient air).

S.5. Cu K-edge X-ray Absorption (XAS)

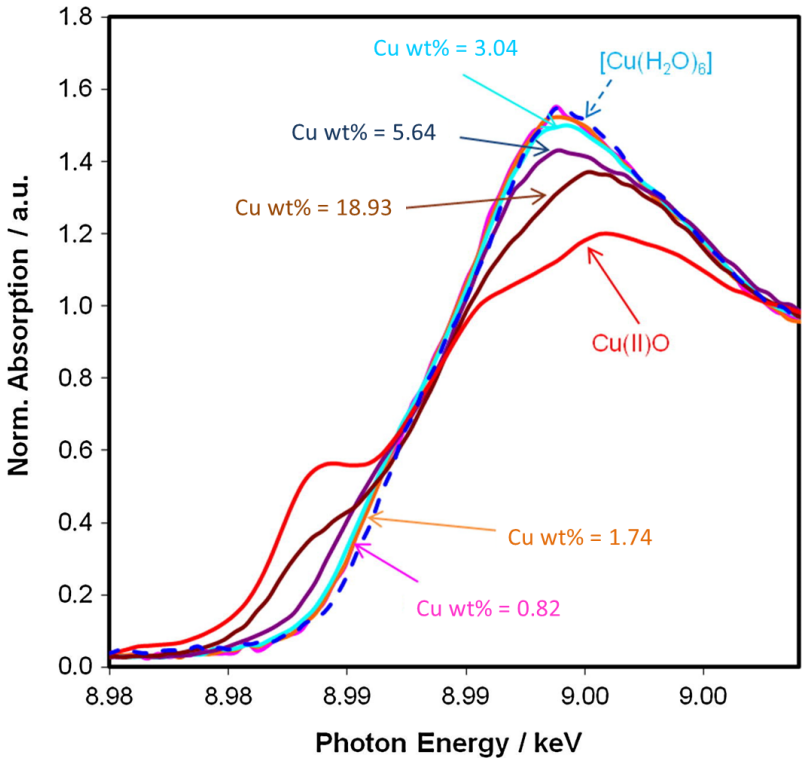

Figure S.4. Ambient Cu K-edge X-ray absorption spectra collected on bulk Cu(II)O (red), aqueous $Cu(NO_3)_2$) (blue), and five Cu-SSZ-13 samples with Cu wt% from 0.82-18.93. All Cu-SSZ-13 materials were Si:Al = 4.5 and were calcined after Cu-exchange then cooled and exposed to ambient air prior to collecting ambient XAS spectra. These data were originally reported in Verma et al. [1].

S.6. Dry NO oxidation kinetics Cu-SSZ-13 catalysts

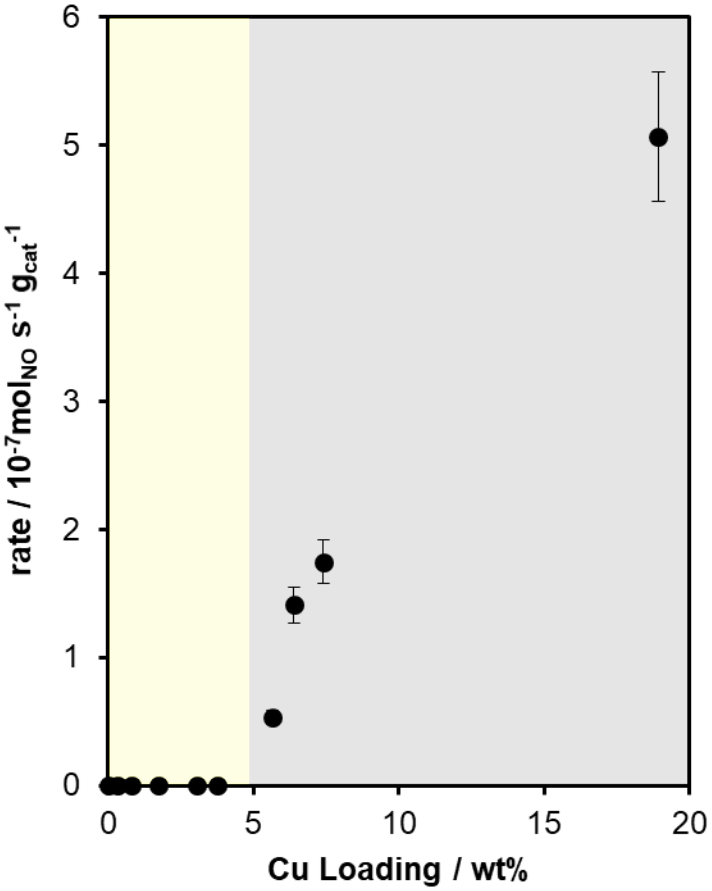

Figure S.5. The dry NO oxidation reaction rate normalized per gram of catalyst plotted versus the Cu wt%. Dry NO oxidation conditions (300 ppm NO, 150 ppm NO_2, 10% O_2, in balance N_2, 543 K). Cu-SSZ-13 catalysts with a Si:Al molar ratio of 4.5 and Cu wt% from 0-19 were synthesized and used for this study. The yellow shaded area between 0 and 4 wt% represents samples with all Cu as ionic Cu^{2+}/Cu^{1+} species. The grey shaded area between 4 to 19 wt% represents samples that contain bulk Cu_xO_y species. Data for all samples except that with Cu wt% 7.40 were originally reported in Verma et al. [1].

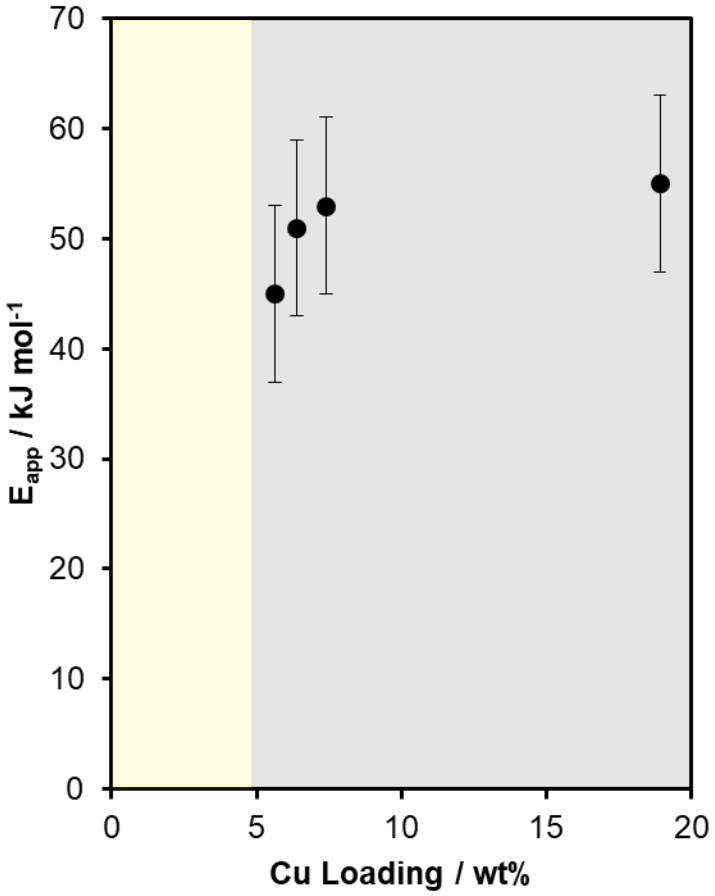

Figure S.6. The dry NO oxidation apparent activation energy plotted versus the Cu wt%. Dry NO oxidation conditions (300 ppm NO, 150 ppm NO_2, 10% O_2, in balance N_2, 543 K). Cu-SSZ-13 catalysts with a Si:Al molar ratio of 4.5 and Cu wt% from 0-19 were synthesized and used for this study. The yellow shaded area between 0 and 4 wt% represents samples with all Cu as ionic Cu^{2+}/Cu^{1+} species. The grey shaded area between 4 to 19 wt% represents samples that contain bulk Cu_xO_y species. Data for all samples except that with Cu wt% 7.40 were originally reported in Verma et al. [1].

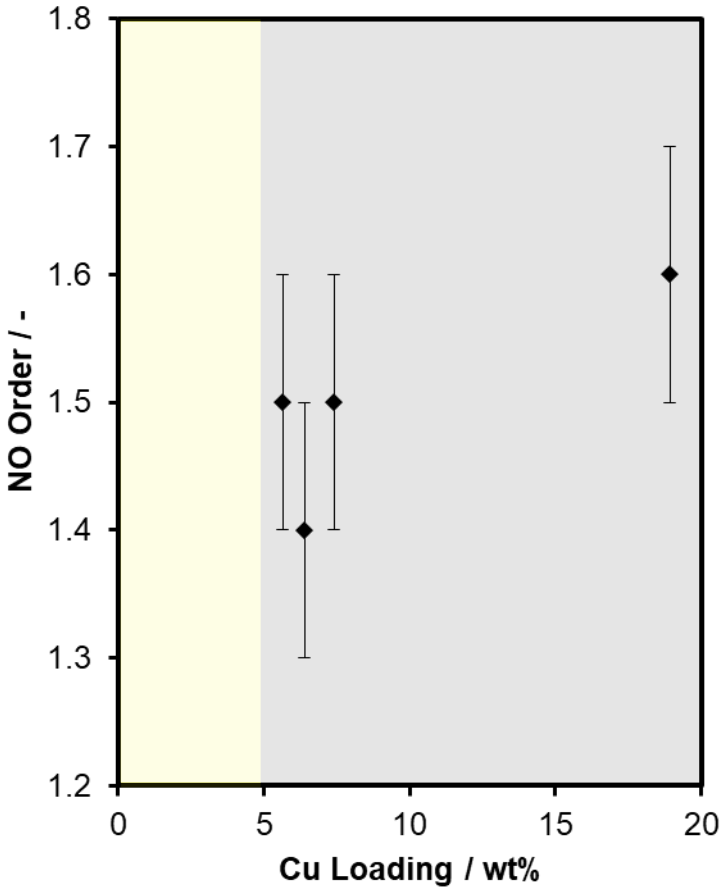

Figure S.7. NO reaction orders plotted versus the Cu wt% under dry NO oxidation conditions (300 ppm NO, 150 ppm NO_2, 10% O_2, in balance N_2, 543 K). Cu-SSZ-13 catalysts with a Si:Al molar ratio of 4.5 and Cu wt% from 0-19 were synthesized and used for this study. The yellow shaded area between 0 and 4 wt% represents samples with all Cu as ionic Cu^{2+}/Cu^{1+} species. The grey shaded area between 4 to 19 wt% represents samples that contain bulk Cu_xO_y species. Data for all samples except that with Cu wt% 7.40 were originally reported in Verma et al. [1].

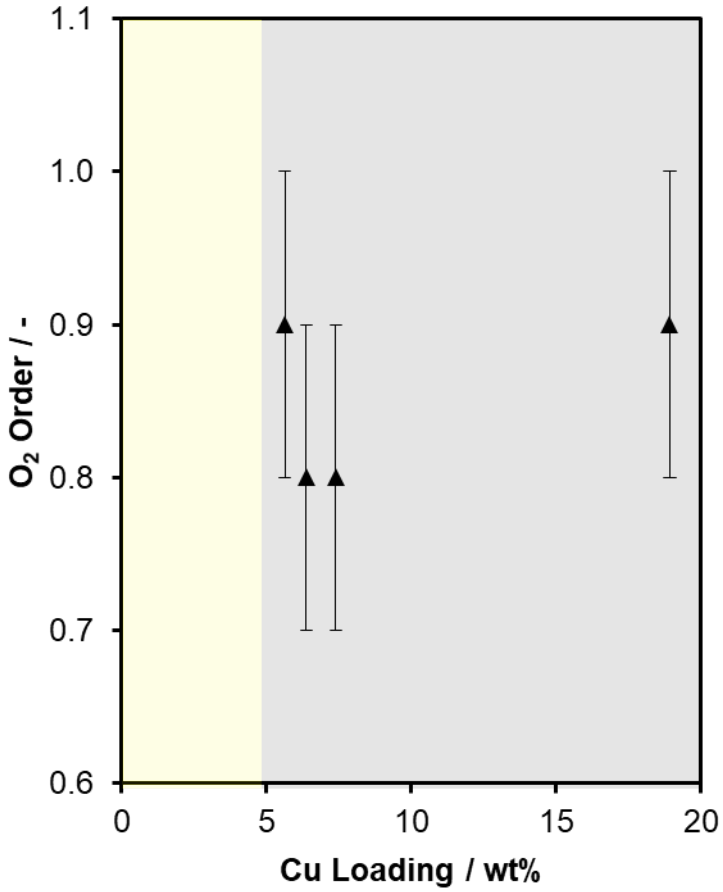

Figure S.8. O_2 reaction orders plotted versus the Cu wt% under dry NO oxidation conditions (300 ppm NO, 150 ppm NO_2, 10% O_2, in balance N_2, 543 K). Cu-SSZ-13 catalysts with a Si:Al molar ratio of 4.5 and Cu wt% from 0-19 were synthesized and used for this study. The yellow shaded area between 0 and 4 wt% represents samples with all Cu as ionic Cu^{2+}/Cu^{1+} species. The grey shaded area between 4 to 19 wt% represents samples that contain bulk Cu_xO_y species. Data for all samples except that with Cu wt% 7.40 were originally reported in Verma et al. [1].

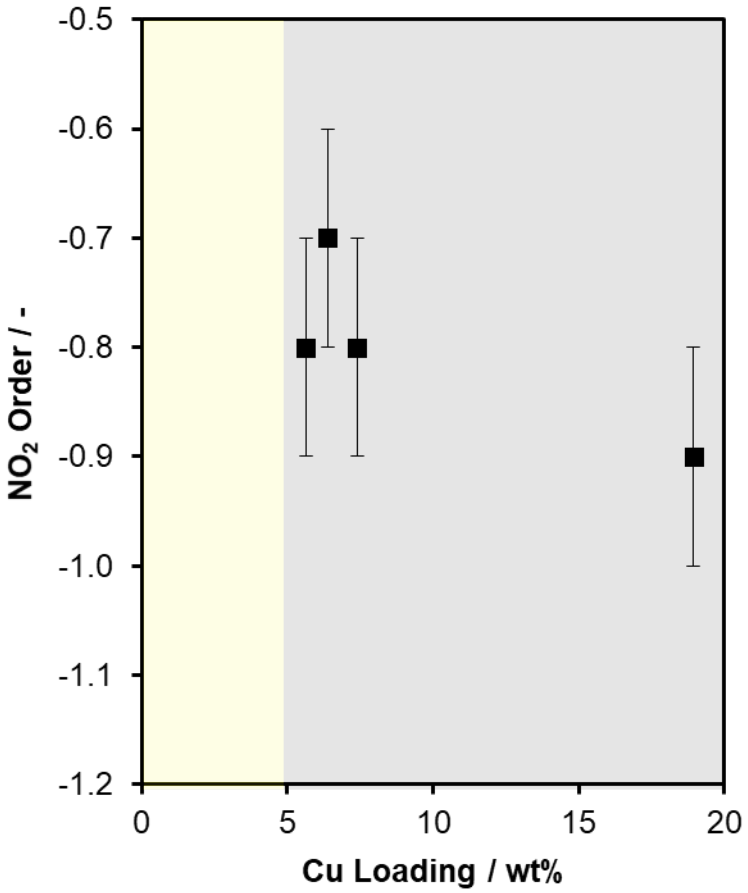

Figure S.9. NO_2 reaction orders plotted versus the Cu wt% under dry NO oxidation conditions (300 ppm NO, 150 ppm NO_2, 10% O_2, in balance N_2, 543 K). Cu-SSZ-13 catalysts with a Si:Al molar ratio of 4.5 and Cu wt% from 0-19 were synthesized and used for this study. The yellow shaded area between 0 and 4 wt% represents samples with all Cu as ionic Cu^{2+}/Cu^{1+} species. The grey shaded area between 4 to 19 wt% represents samples that contain bulk Cu_xO_y species. Data for all samples except that with Cu wt% 7.40 were originally reported in Verma et al. [1].

S.7. Relaxation of differential assumption for PFR

Here, we relax the approximation that the PFR is differential and numerically integrate the PFR equations in Eq. 2 for the rate with the values of *a*, *b*, and *c* of 1.5/(1-(-0.9)), 1.1/(1-(-0.9)), and -0.9, respectively, extracted from the co-feeding analysis in Section 4.1. We start with equation 2:

$$r_{fwd}=k_{eff}\left([NO]_0(1-X)\right)^a([O_2]_0-[NO]_0X/2)^b([NO_2]_0+[NO]_0X)^c \quad \text{(Eq. 2)}$$

And we note that $[NO_2]_0$ is equal to zero, giving:

$$r_{fwd}=k_{eff}\left([NO]_0(1-X)\right)^a([O_2]_0-[NO]_0X/2)^b([NO]_0X)^c \quad \text{(S.1)}$$

or,

$$r_{fwd}=k_{eff}\left([NO]_0(1-X)\right)^{0.79}([O_2]_0-[NO]_0X/2)^{0.58}([NO]_0X)^{-0.9} \quad \text{(S.2)}$$

We reintroduce equation 4, the design equation for a PFR.

$$\tau=[NO]_0\int_0^X \frac{dX}{r_{fwd}} \quad \text{(Eq. 4)}$$

In the main text, we next simplified equation S.1 by assuming small X, but here we will not make this simplification. Therefore:

$$\tau=[NO]_0\int_0^X \frac{dX}{k_{eff}\left([NO]_0(1-X)\right)^{0.79}([O_2]_0-[NO]_0X/2)^{0.58}([NO]_0X)^{-0.9}} \quad \text{(S.3)}$$

Next, we integrate this expression numerically to give the trend in X with respect to τ shown in Figure S.10.

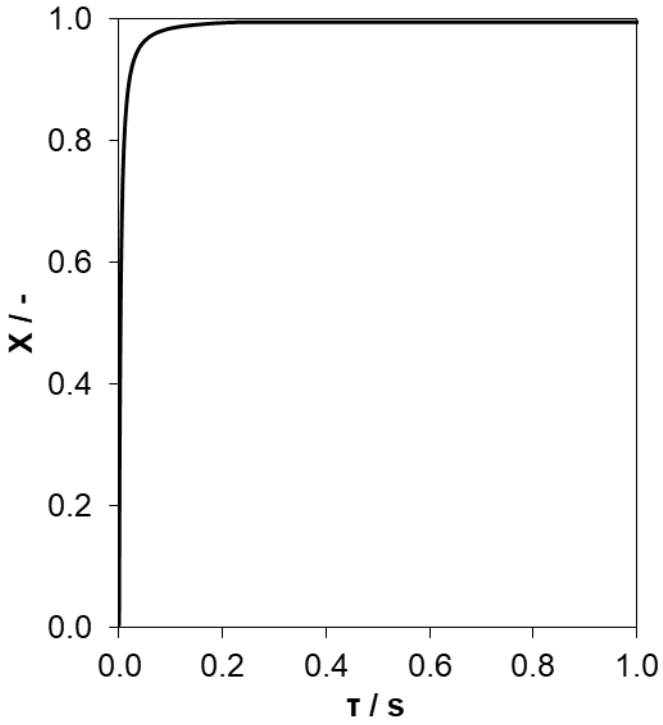

Figure S.10. Conversion as a function of τ as determined by numerical integration of Eq. S.3 using trapezoid rule with 200 mesh points.

We find that the exponent of k_{eff} will lead to apparent activation energies in agreement with those from the co-feeding experiment. For instance, if we vary the value of k_{eff} and then plot the value of X observed at fixed τ, we find that k_{eff} has an exponent of ~0.5187. Now, the expected value is k_{eff} raised to a power of 1/(1-c), and in this case c is -0.9, giving k_{eff} raised to 0.53, which is similar to the exponent shown in in Figure S.11.

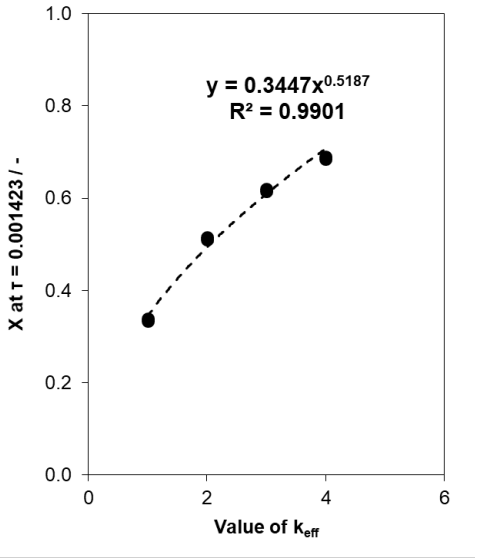

Figure S.11. Conversion at a fixed value of τ as a function of k_{eff}.

S.8. Derivation of equation 10

From the definition of the equilibrium constant, K:

$$K=\exp\left(\frac{-\Delta G_B^\circ}{RT}\right) \quad (S.4)$$

With ΔG_B° as the free energy for adsorption of B. When $K_B P_B=0.1$, as was assumed in Section 5.2, we can solve for P_B in terms of thermodynamic quantities as follows:

$$K_B P_B=0.1 \quad (S.5)$$

Combining equations S.4 and S.5 gives:

$$\exp\left(\frac{-\Delta G_B^\circ}{RT}\right) P_B=0.1 \quad (S.6)$$

Rearranging equation S.6 and substituting for ΔG:

$$P_B=0.1\exp\left(\frac{\Delta H_B^\circ - T\Delta S_B^\circ}{RT}\right) \quad (S.7)$$

Where ΔH_B° and ΔS_B° are the enthalpy and entropy of adsorption of B. For adsorption of B with $-\Delta S_{ads}$ assumed to be 105 J (mol K)$^{-1}$, this equation simplifies to:

$$P_B=0.1\exp\left(\left(105+\frac{\Delta H_B^\circ}{T}\right)R^{-1}\right) \quad (10)$$

Which is equation 10.

S.9 Range of parameter space where errors from neglecting product inhibition are significant

In the main text, an approximate entropy value of 84 kJ mol^{-1} was used. In this section, we discuss the effect of the enthalpy and entropy of product adsorption on the measured rate in the context of a simple example, the irreversible surface-catalyzed reaction of A→B. The set of elementary steps we will use are as follows:

1. $A + * \leftrightarrow A*$
2. $A* \rightarrow B*$
3. $B + * \leftrightarrow B*$

Step 1 and 3 are assumed to be quasi-equilibrated, and step 2 is considered the sole rate limiting step, and we consider vacant sites (*) and adsorbed species B (B*) as the most abundant surface intermediates (MASI), which can result in inhibition by species B depending on the magnitude of K_3P_B. Those assumptions result in the following rate law, r_{inh}, for the case that B inhibits the reaction:

$$r_{inh}=\frac{k_2K_1P_AL}{1+K_3P_B} \quad \text{(S.8)}$$

Where K_1 and K_3 are the equilibrium constants for steps 1 and 3, k_2 is the rate constant for step 2, L is the total number of active sites, and P_A and P_B are dimensionless pressures for species A and B, respectively. We can then derive an expression for the case that product inhibition is neglected, in which case at low pressures where the coverage of A is considered low and vacant sites are the sole MASI and the rate expression for the uninhibited reaction, run, is given by:

$$r_{un}=k_2K_1P_AL \quad \text{(S.9)}$$

The relative percent error between the measured rates is given by:

$$\%\ \text{error in measured rate}=\frac{100*(r_{un}-r_{inh})}{r_{inh}} \quad \text{(S.10)}$$

Based on the form of eq. S.10, we need not specify a value for $k_2K_1P_AL$, as this term fortuitously cancels upon further simplification of eq. S.10.

And finally, from thermodynamics we know that K_3P_B is equivalent to:

$$K_3P_B=P_B\cdot\exp\left(\frac{-\Delta H^{\circ}_{ads,B}}{RT}\right)\cdot\exp\left(\frac{\Delta S^{\circ}_{ads,B}}{R}\right) \quad \text{(S.11)}$$

In Figure S.12, we show the impact of inhibitory product pressure and the adsorption enthalpy of the inhibitory product on the error that results when product inhibition is ignored. Each of the three rows illustrates the error in the rate using a different enthalpy-dependent formula for the adsorption entropy, as discussed in section 5.2 of the main text. The magnitude of the entropy loss upon adsorption increases going from the bottom row to the top row. As expected for exothermic adsorption events, the error is less significant for all pressures and adsorption enthalpies at higher temperatures, reflecting decreases in the coverage of the inhibitory product. Assuming a feed of 100% of A at atmospheric pressure, a reactor temperature of 600 K, and 10 percent conversion of

A (10 kPa B formed), inhibition would result in ten percent error or more if the negative adsorption enthalpy were ~50 kJ mol^{-1} or higher, using the lower bound estimate for the entropy of adsorption of -41.8 J mol^{-1} K^{-1}.

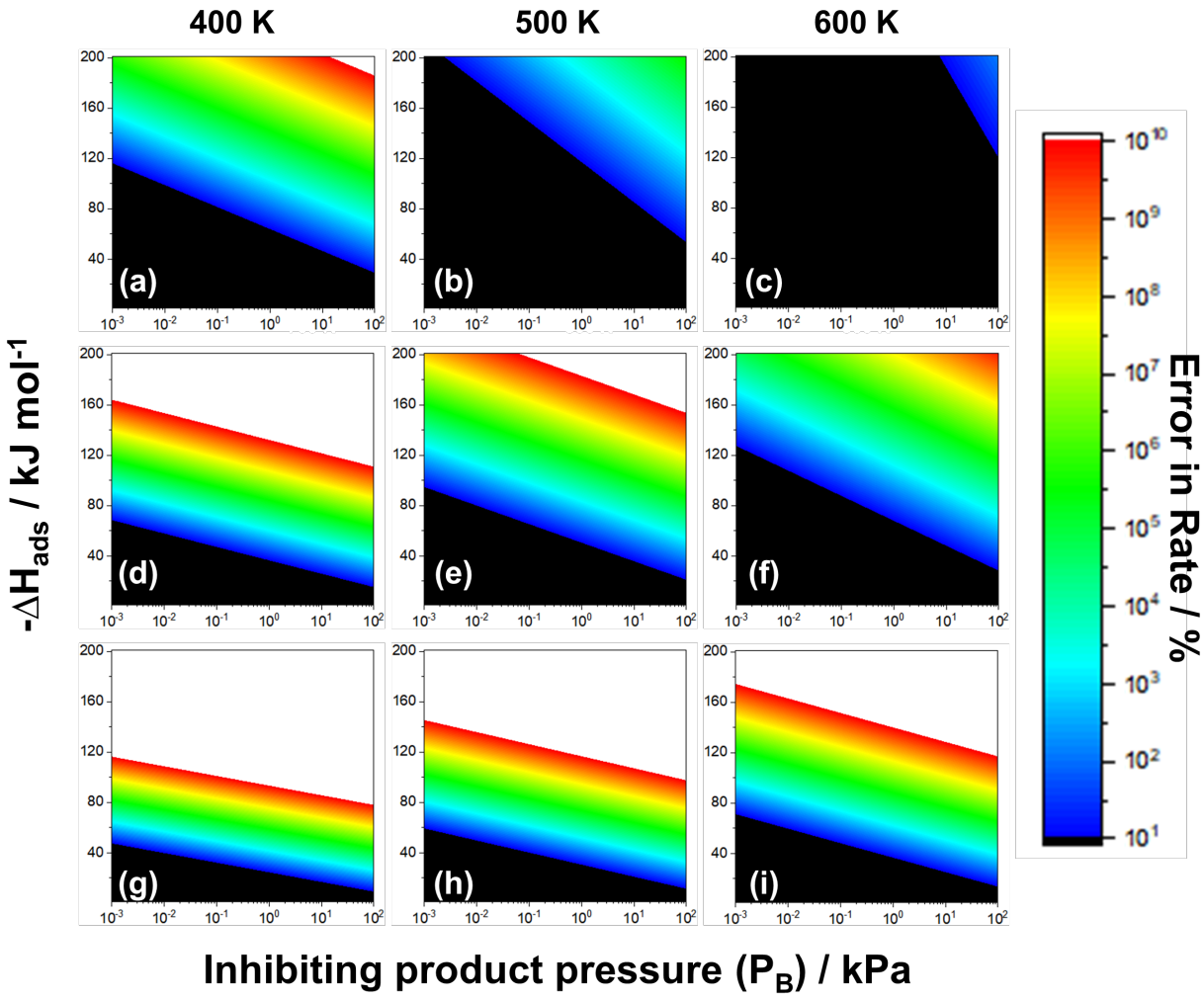

Figure S.12. Percent difference in the rate of reaction when product inhibition is not included in the rate expression, as a function of the pressure of the inhibiting product (B) and the enthalpy of adsorption of species B. Plots (a)-(c) use the upper bound for entropy of adsorption as reported by Vannice et al. [2] (see Section 5.2 of the main text,), plots (d)-(f) use the average of the upper bound and lower bound adsorption entropy, and plots (g)-(i) use the lower bound for adsorption entropy (-41.8 J mol^{-1} K^{-1}) at 400 K (a,d,e), 500 K (b,e,h), and 600 K (c, f, i).

S.10 Derivations for Section 5.2

The full rate law given by Verma et al. [1] is:

$$-r_{NO}=\frac{k_2K_1L[NO]^2[O_2]}{[NO]+K_3^{-1}K_4^{-1}[NO_2]+K_1[NO][O_2]+K_4^{-1}[NO][NO_2]} \quad \text{(S.12)}$$

Where the rate and equilibrium constants refer to the steps from Scheme 1 in the main text. If the numerator and denominator of the equation S.12 are multiplied by (*), the first term in the resulting denominator the coverage of vacant sites (*), the second term is the coverage of O*, the third term is the coverage of O_2*, and the fourth term is the coverage of NO_2*. Given the near unity reaction order for oxygen reported in Figure 2, we conclude that the coverage of O_2* is ~0. With that assumption, the rate law becomes:

$$-r_{NO}=\frac{k_2K_1L[NO][O_2]}{1+\frac{K_3^{-1}K_4^{-1}[NO_2]}{[NO]}+K_4^{-1}[NO_2]} \quad \text{(S.13)}$$

By taking the derivative of the natural log of the rate with respect to the natural log of the concentration of each species in the system[1], the reaction orders with respect to NO, O_2, and NO_2 reflect the coverages of these intermediates as defined in equations S.14-S.16:

$$n_{NO}=2-\theta_*-\theta_{NO_2^*} \quad \text{(S.14)}$$

$$n_{O_2}=1 \quad \text{(S.15)}$$

$$n_{NO_2}=-(\theta_{O^*}+\theta_{NO_2^*}) \quad \text{(S.16)}$$

Based on the measured reaction orders for NO, O_2, and NO_2 of 1.5±0.1, 1.1±0.1, and -0.9 ± 0.1, respectively, we calculate that the coverage of NO_2 is 0.4, the coverage of O* is 0.5, and the coverage of * is 0.1, resulting in the required sum of coverages of one. This coverage of NO_2^*, measured here at 543 K, is twice as high as that reported by Verma et al. [1] for measurements performed at 573 K, and the coverage of O* reported here is slightly smaller (by 0.1) than that reported by Verma et al., while the coverage of * is identical in both cases. The coverage of O_2* is zero here, whereas it was 0.1 in Verma et al. [1]. A higher coverage of NO_2* would be expected given the lower reaction temperature used in this study. In summary, the reaction orders measured in this study are consistent with the rate expression reported in S.13 and eq. 12 in the main text and with the results of Verma et al. [1].

The elementary steps proposed by Metkar et al. [3] are given in Scheme S.1.

1. $O_{2(g)} + * \leftrightarrow O_2^*$

2. $O_2^* + * \leftrightarrow 2O^*$

3. $NO_{(g)} + O^* \leftrightarrow NO_2^*$

4. $NO_{2(g)} + * \leftrightarrow NO_2^*$

Scheme S.1. Series of elementary steps reported by Metkar et al. [3],.

We note that this scheme is not consistent with our data, because it cannot give NO orders greater than 1. Steps 3 and 4, however are the same as steps 3 and 4 in our scheme 1, but we have assumed that step 3 is quasi-equilibrated as well as step 4. Metkar et al. assumed steps 1, 2, and 4 in Scheme 1 were equilibrated. Using the steps in Scheme S.1, the following definitions were reported by Metkar et al. [3]: $K_i = \frac{k_{f,i}}{k_{b,i}}$ (S.17)

Where $k_{f,i}$ is the forward rate constant for step i and $k_{b,i}$ is the reverse rate constant for step. Each rate constant is defined as:

$$k_i = A_i * \exp\left(\frac{-E_i}{RT}\right) \quad \text{(S.18)}$$

where A_i is the pre-exponential factor, E_i is the activation energy for each step, R is the ideal gas constant (8.314 J mol^{-1} K^{-1}), and T is the temperature in K.

Thus, based on eqs. S.17 and S.18, K_4/K_3 is given by:

$$\frac{K_4}{K_3} = \frac{A_{f,4} * \exp\left(\frac{-E_{f,4}}{RT}\right) \Big/ A_{b,4} * \exp\left(\frac{-E_{b,4}}{RT}\right)}{A_{f,3} * \exp\left(\frac{-E_{f,3}}{RT}\right) \Big/ A_{b,3} * \exp\left(\frac{-E_{b,3}}{RT}\right)} \quad \text{(S.19)}$$

The given values for $A_{f,3}$, $A_{b,3}$, $A_{f,4}$, $A_{b,4}$, E_{f3}, $E_{b,3}$, $E_{f,4}$, and $E_{b,4}$ from Metkar et al. [3] are reported in Table S.2.

Table S.2. Values for pre-exponential factors and activation energies reported by Metkar et al. [3].

Step (i)	**Pre-exponential factor, A_i mol $m^{-3}_{washcoat}$ s^{-1}**	**Activation energy, E_i kJ mol^{-1}**
f,3	$6.41 \pm 0.6 * 10^5$	29.11±5
b,3	$6.38 * 10^{14}$	165.41±5
f,4	$4.33 \pm 1 * 10^6$	0
b,4	$3.41 * 10^{14}$	141.5

Using the values from Table S.2 and eq. S.17, the computed value of K_4/K_3 is:

$$\frac{K_4}{K_3}=12.7\exp\left(\frac{5200}{RT}\right) \quad \text{(S.23}$$

We note that step 4 was written in the opposite direction by Verma et al. [1], such that the left hand side of eq. S.23 would be $K_3^{-1}K_4^{-1}$ using the notation of Verma et al. that is also used here in the main text.

We can also compute the value of K_4^{-1} itself, using the notation of Verma et al. [1], based on the values reported by Metkar et al. [3] in Table S.2:

$$K_4=\frac{k_{f,4}}{k_{b,4}}=\frac{A_{f,4}*\exp\left(\frac{-E_{f,4}}{RT}\right)}{A_{b,4}*\exp\left(\frac{-E_{b,4}}{RT}\right)}=1.27*10^{-8}*\exp\left(\frac{141500}{RT}\right) \quad \text{(S.24)}$$

S.11 References

[1] A.A. Verma, S.A. Bates, T. Anggara, C. Paolucci, A.A. Parekh, K. Kamasamudram, A. Yezerets, J.T. Miller, W.N. Delgass, W.F. Schneider, F.H. Ribeiro, NO oxidation: A probe reaction on Cu-SSZ-13, *J. Catal.*, 312 (2014) 179-190.
[2] M.A. Vannice, S.H. Hyun, B. Kalpakci, W.C. Liauh, Entropies of adsorption in heterogeneous catalytic reactions, *J. Catal.*, 56 (1979) 358-362.
[3] P.S. Metkar, V. Balakotaiah, M.P. Harold, Experimental and kinetic modeling study of NO oxidation: Comparison of Fe and Cu-zeolite catalysts, *Catal. Today*, 184 (2012) 115-128.